

Effects of Thermal Treatment on Laser Generated Aerosols using LA-ETV-ICP-MS

Tomas Vaculovic^a, Marcel Guillong^b, Jürg Binkert^b, Viktor Kanicky^a and Detlef Günther^{b*}

Contribution from: ^aLaboratory of Atomic Spectrochemistry, Faculty of Science, Masaryk University in Brno, Kotlářská 2, CZ 611 37 Brno, Czech Republic; ^bLaboratory of Inorganic Chemistry, ETH, Hönggerberg HCI G113, Wolfgang-Pauli-Strasse 10, CH-8083 Zürich, Switzerland.

Received: August 30, 2004

Accepted (in revised form): December 8, 2004

Résumé

La distribution de grandeurs de particules d'un aérosol est généralement connu comme étant critique pour la vaporisation complète d'un échantillon par introduction dans une décharge ICP. La dépendance de la composition sur la grandeur de particules d'un aérosol produit avec un laser a été prouvée comme étant responsable de la fractionation élémentaire induite par l'ICP. La modification de la distribution de grandeurs de particules a été étudiée en chauffant l'aérosol généré par un laser au moyen d'un vaporisateur électrothermique (ETV) installé entre la cellule d'ablation et la torche d'ICP. En tout, 21 cibles de métaux simples furent ablatées et chauffées par l'ETV avant d'entrer dans la décharge ICP. De plus, des échantillons de laiton et d'acier furent étudiés comme échantillons multiélémentaires. Le but de cette étude était a) de modifier la distribution de grandeurs de particules vers des diamètres réduits; b) de déterminer la dépendance élémentaire du processus de vaporisation, et c) de déterminer la séparation de phase, en différentes grandeurs de particules, induite par le laser et dépendant de chaque élément.

Il fut observé que la vaporisation dépendait des points de fusion des métaux, et la distribution de grandeur de particule pouvait être réduite pour les éléments à bas points de fusion. Les expériences d'ablation avec des échantillons de laiton et d'acier révélèrent que quelques éléments étaient séparés en grandeurs de particules individuelles. Les signaux

originaux de particules produites par ablation d'une cible de zinc se comportèrent, dans l'ETV, similairement aux signaux de Zn générés par du laiton. Ces études peuvent être utilisées pour indiquer la manière dont une particule se vaporise dans l'ICP, même si les températures utilisées dans l'ETV sont plus basses que dans un ICP.

Abstract

Aerosol particle size distribution is generally known to be critical for complete sample vaporization upon introduction into an ICP discharge. Particle size dependent composition of laser-produced aerosols has been proved to be responsible for ICP-induced elemental fractionation. The modification of the particle size distribution has been studied based on heating a laser-generated aerosol by means of an electrothermal vaporizer (ETV) installed between an ablation cell and an ICP torch. Overall, 21 single-metal targets were ablated and heated up by the ETV prior to entering into the ICP discharge. Brass and steel samples were also studied as multielement samples. The aim of this study was a) to modify the particle size distribution towards reduced diameters b) to determine the elemental dependence of the vaporization process, and c) to determine element-dependent laser-induced phase separation into different particle sizes.

It was observed that the vaporization depended on melting points of metals, and the particle size distribution could be reduced for low-melting elements. Ablation experiments with brass and steel

* Author to whom correspondence should be addressed: guenther@inorg.chem.ethz.ch

samples revealed that some elements were separated into individual particle sizes. Signals originating from particles produced by ablation of a zinc target behave similarly in the ETV to Zn signals generated in brass. These studies can be used to indicate the particle vaporization behaviour within the ICP, even knowing that the temperatures used within the ETV are lower than in an ICP.

Keywords: LA-ICP-MS, aerosols, ETV, elemental fractionation

Introduction

Electrothermal vaporization (ETV) is well known in the form of the graphite furnace (GF) in atomic absorption spectroscopy (AAS), where it has served as a good source of atoms (electrothermal atomizer – ETA) for more than 25 years (1). The first combination of an ETV with an ICP was reported in 1974 (2). Moreover, the use of ETV as a sampling device for ICP spectroscopy has been widely reported during the last 15 years. ETV has been used for the analysis of biological samples (3-5), geological materials (6-8), and alloys (9,10). Analyte transport in ETV-ICP-MS is affected by significant losses, which occur at transfer in the tube and on the switching valve, and can be as high as approximately 75 % (11) for solutions. In the case of solid sampling, a transport efficiency of up to 35 % for Pb was achieved (12).

Laser ablation solves many of the problems associated with the dissolution of solid samples, diminishes some of interferences, such as ArO^+ , and reduces contamination, while providing good detection limits. However, one of the limitations of the ablation of solid samples is the observation of selective elemental fractionation related to the different melting temperatures of the various sample components of the sample. The selective fractionation is affected by the ablation parameters used, including laser wavelength, repetition rate, pulse width, fluency (13,14), and transport parameters (15).

Particles play an important role in LA-ICP-MS because the particle formation processes including nucleation, condensation, and agglomeration can significantly affect analytical performance (16-19). Observation of the fluctuations of ICP-MS or ICP-OES signals suggests the influence of the particles. Particles larger than $0.5 \mu\text{m}$ are not completely converted to ions in the ICP and are one of the important causes of a matrix

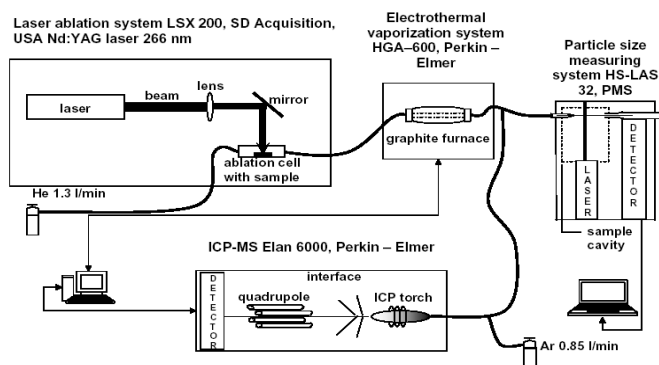


Figure 1. Schematic of the experimental setup

effect (20).

The aim of this study is to investigate the influence of ETV temperatures on the particle size distribution and on ICP-MS signals from metallic samples containing only one element (for example Al, Cr, Cu, Zn, etc.) in comparison to multielement alloy samples (brass and steel). As well, the purpose of this study is to compare the behaviour of the metals in the multielement samples with their behaviour in single-element samples. This work also investigates the use of an ETV to decrease the total volume of the particles reaching the ICP, which could result in a decrease of ICP-induced fractionation.

Experimental

In order to study the behaviour of particles transported to the ICP, an online electrothermal vaporization unit (ETV) was installed between a laser ablation cell and the ICP-MS (Figure 1). A 266 nm Nd:YAG laser system (Laser ablation system LSX 200) was used to produce the ablated material. The laser was operated at a 5 Hz repetition rate, using an energy density of 30 J cm^{-2} . The crater diameter was $25 - 50 \mu\text{m}$. The ablation was carried out using a scan rate of $5 \mu\text{m s}^{-1}$. Laser ablation parameters are given in Table 1. The laser-produced aerosol was transported in helium through the ETV (Electrothermal vaporization system HGA-600, Perkin-Elmer, Canada). The ETV system was made of pyrolytic coated graphite. Two temperature programs were used (Figure 2). The first temperature program was used to measure the ICP-MS signal intensities (Figure 2). The graphite tube was heated to $2700 \text{ }^\circ\text{C}$ in 100 s. The temperature was held for 5 s and then decreased over 100 s. A second temperature program was used for monitoring the change in the ICP-MS signal intensity and

Table 1. Laser ablation parameters

Laser system parameters	LSX 200
Type	Nd:YAG
Wavelength	266 nm
Spot size	25 - 50 μm
Energy density	30 J/cm ²
Scan rate	5 $\mu\text{m/s}$
Repetition rate	5 Hz
Carrier gas	He
Flow rate	1.3 L/min

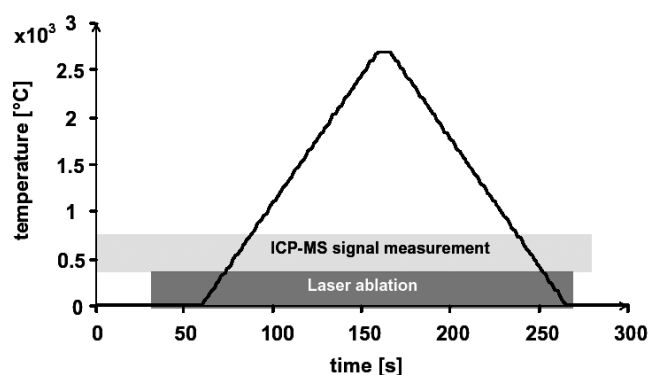


Figure 2. Temperature program used only for ICP-MS signal intensity measurement.

for particle size distribution measurement (Figure 3). In this temperature program, the graphite tube was held at 20°C for 60 s. Then it was heated to 2400°C in 5 s, held at this temperature for 60 s, and then the temperature was decreased to ambient in 5 s. The temperatures reported were those programmed into the ETV controller, but no experimental attempts were made to determine the actual wall or gas temperature. It is likely that the gas temperature may be significantly lower than the wall temperature (21), which may also be lower than the set temperature because of the cooling effect of the flowing gas stream.

The heated aerosol was carried in helium gas (1.3 L min⁻¹). This gas stream was split, with one part going to the ICP-MS for intensity measurement (ICP-MS Elan 6000, Perkin-Elmer, Canada). The second part of the aerosol stream went to a particle size measuring system (HS-LAS, PMS, USA). This device measured the particle size distribution in a range of 0.05 to 1 μm . The particle

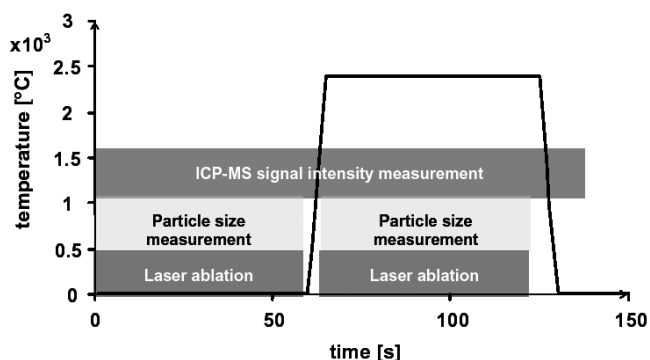


Figure 3. Temperature program used for ICP-MS intensity signal and particle size distribution measuring.

size distribution measurement was carried out for 60 s, after which the sample particulate volume was calculated for each channel, assuming spherical particles (22).

Twenty-one single element metallic samples (Ag, Al, Au, Bi, Cd, Co, Cr, Cu, Ga, Mg, Mn, Mo, Ni, Pb, Pt, Si, Sn, Ta, Ti, W, and Zn) were ablated using a fluence of 30 J cm⁻², a crater size of 25 to 50 μm , in scanning mode at 5 $\mu\text{m s}^{-1}$, with a repetition rate of 5 Hz. Further, three steel samples (520, 522, 533 from Kralovopolska Brno, Czech Republic), a stainless steel (CRM JK37), and a brass (MBH 31XB22) were ablated using the same ablation conditions.

Results and Discussion

Influence of the ETV temperature program on the ICP-MS signal intensity in single element samples

The recording of the ICP-MS signal intensities and the ETV temperature program were started simultaneously. Laser firing was then started after 30 s (Figure 2). During the heating of the graphite furnace, there was an initial decrease in the ion signal intensities, followed a subsequent increase. The temperature at which the signal intensity inflection occurred was different for each element. However, for the metals which have high vaporisation temperatures (Mo, Ta, W), no inflection in the ion signal was observed (Figure 4). To quantitatively interpret the observed pattern of signal changes, the temperature at which the decrease started was determined from a mathematical analysis of the intensity vs time data. The inflection temperature was obtained using a tangential method (Figure 5). Three straight lines and their equations were calculated:

$$\alpha) I_1 = a_1 t + b_1,$$

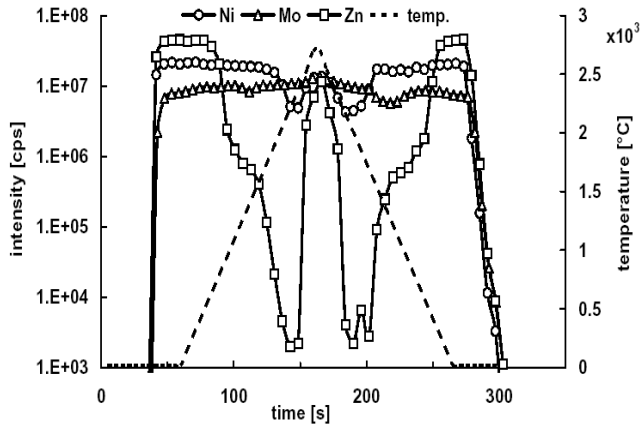


Figure 4. Transient signal for single element ablations during ETV heating

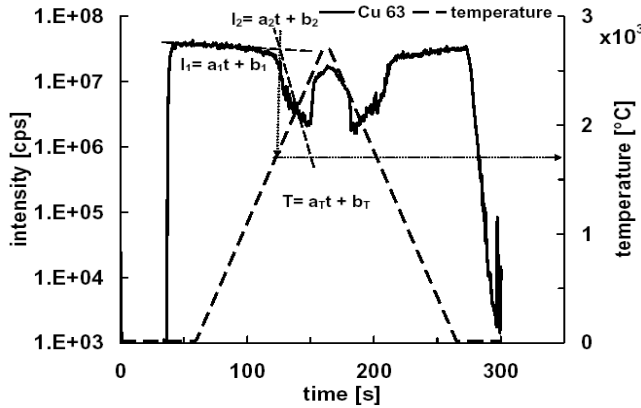


Figure 5. Calculation of the temperature, where the signal intensity starts to decrease

$$\beta) I_2 = a_2t + b_2,$$

$$\gamma) T = a_Tt + b_T$$

where I_1 and I_2 are the intensities of the ICP-MS signal, t is time, and T is temperature. At the point of intersection of the two equations α and β it follows that:

$$t = (b_2 - b_1) / (a_1 - a_2) \text{ and } T = a_T(b_2 - b_1) / (a_1 - a_2) + b_T$$

The point where the lines shown in Figure 5 intercept will be termed the “onset” time and temperature. The calculated onset temperatures are summarized in Table 2.

Figure 6 shows the correlations between determined onset temperatures, the boiling points, and the melting points of metals.

Table 2. Calculated temperature of the start of decreasing ICP-MS intensity, boiling and melting point of ablated metals.

Element	Calcul. temp [°C]	Boiling point [°C]	Melting point [°C]
Cd	582±19	767	321
Zn	704±26	907	420
Mg	1035±31	1090	650
Pb	1307±49	1749	327
Al	1523±36	2519	660
Ga	1537±33	2204	30
Mn	1583±30	2061	1246
Ag	1677±45	2162	962
Cu	1718±18	2927	1085
Sn	1768±68	2602	232
Si	1900±38	2900	1414
Co	1944±24	2927	1495
Cr	1981±21	2671	1907
Ni	2010±46	2913	1455
Au	2087±62	2856	1064
Ti	2417±32	3287	1668

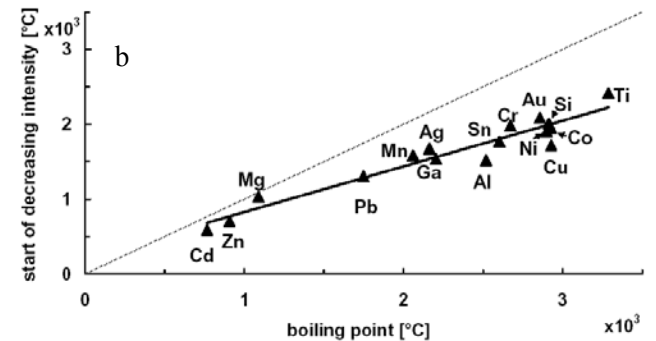
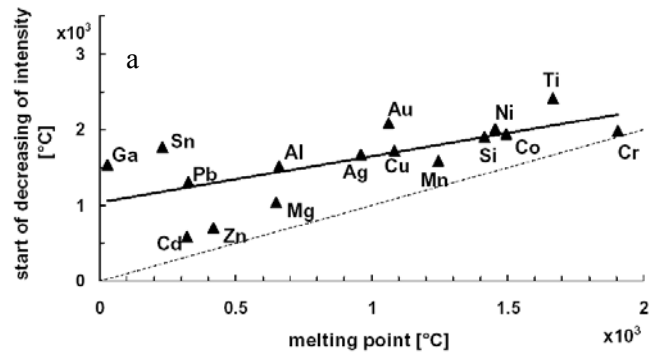


Figure 6. a: Correlation between removal temperature and melting point; (- - -) unity slope. b. Correlation between removal temperature and boiling point; (- - -) unity slope

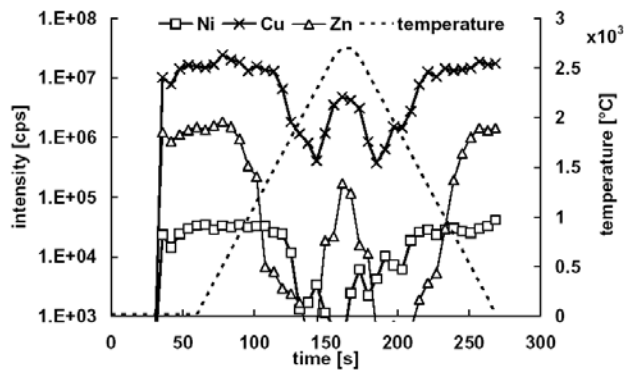


Figure 7. Transient signal for brass

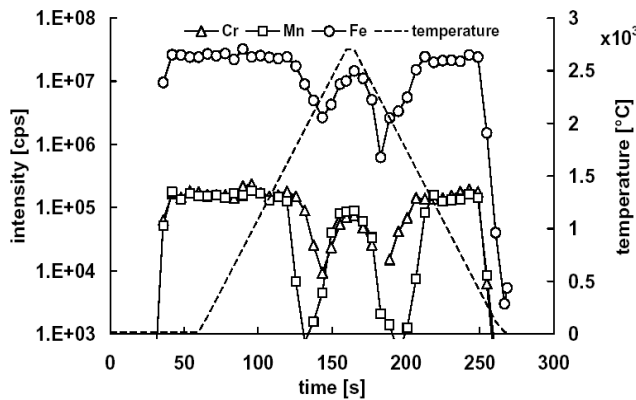


Figure 8. Transient signal for steel

Influence of the ETV temperature program on the ICP-MS signal intensity in multielement samples

The ablation parameters for the alloys were the same as for the single element samples. Samples of brass and steel were ablated, and the time resolved ion signal was obtained (Figure 7 and 8). The observed signal behaviour in these brass and steel samples was similar to that obtained from the single element samples. However, there were differences in the temperature at which the intensity onset occurred.

In the brass sample (Figures 7, 9b), the Zn signal intensity starts to decrease at the same temperature as was observed for a sample containing only Zn. For the Cu signal in the same sample, the decrease occurs at a lower temperature. This suggests that only Zn forms a separate phase (Figure 9a and b). Strongly decreased onset temperatures are observed for Ag, Pb, Al and Sn. It is possible that these metals are alloyed in the Cu phase, while Mn and Ni (slightly decreased onset temperatures) are alloyed in Zn phase.

For the steel sample (Figures 8, 9c), most elements'

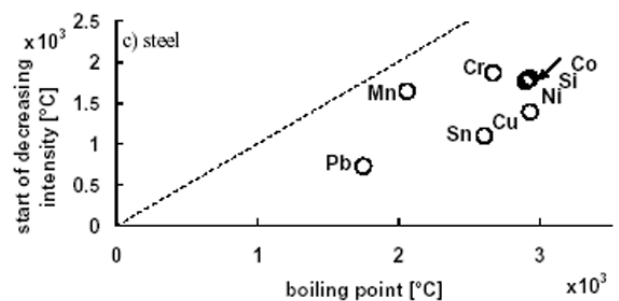
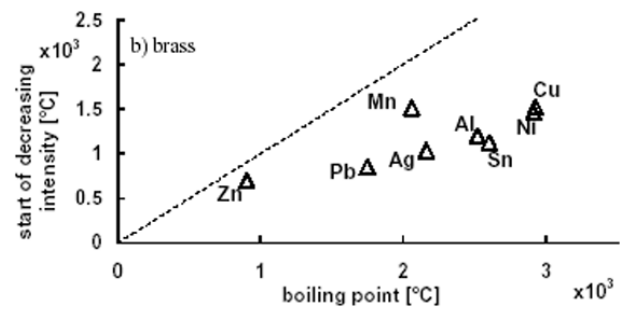
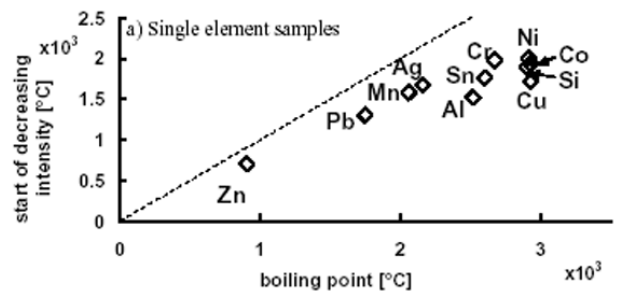


Figure 9. Correlation between removal temperature and boiling point for single element samples (a), brass (b) and steel (c); (---) unity slope

(Cr, Si, Mn, Ni, Co, Mo, and W) signal intensities do not follow the single element onset temperatures. This suggests that these metals are not phase-separated, and these particles remained alloyed with the Fe.

The processes affecting the aerosol when it passes through the ETV as well as the cause of the initial decrease and the subsequent increase in signal intensity during the heating cycle require explanation. The model proposed here is that the ablated material is heated while passing through the furnace. At a certain temperature, approximately 500°C below the boiling point of the metal, aerosol evaporation commences. Unfortunately, since the exact temperature in the tube is unknown, the vaporization temperature cannot be given. Measurements given in reference (23), however, indicate that the temperature

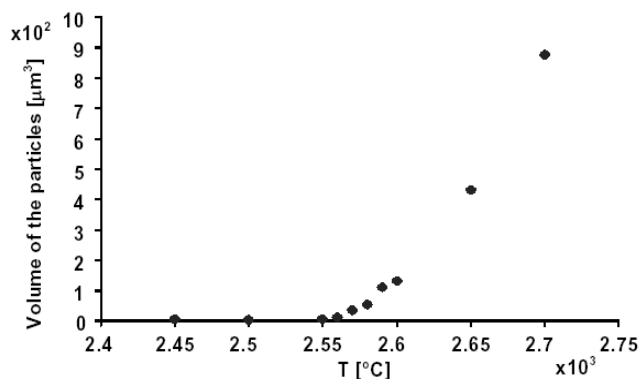


Figure 10. Temperature dependent carbon particle release from graphite furnace

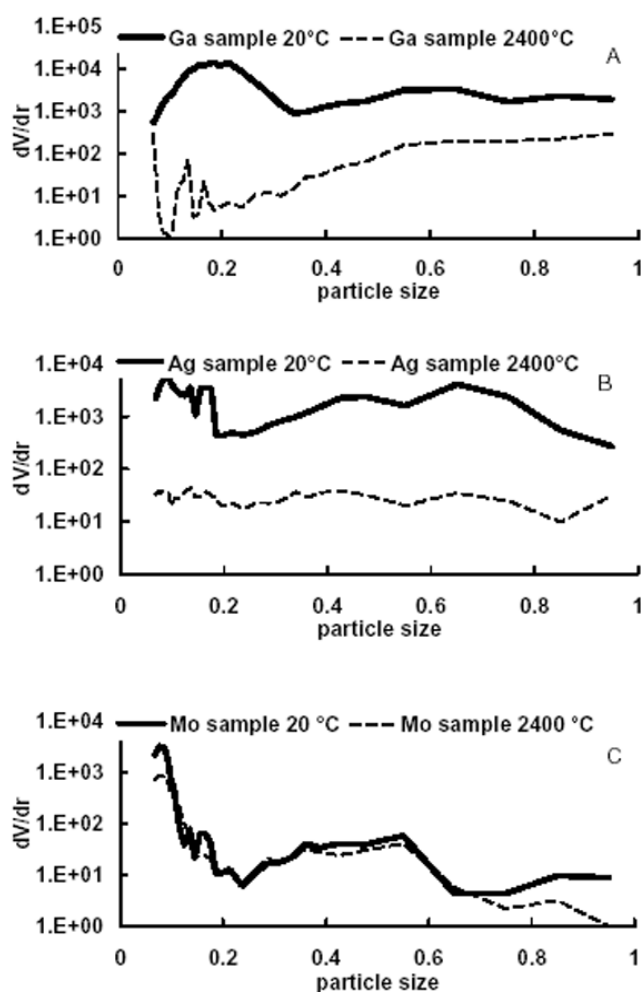


Figure 11. Influence of different temperature on particle size distribution (particle size given in μm) of gallium (A), silver (B) and molybdenum (C)

can decrease by 300 °C when using a 1 L/min Ar flow through the ETV. The created vapour is then adsorbed on the surface of the transfer tube from the ETV to the ICP or due to the temperature gradient within the graphite tube (23), resulting in a decrease in the observed signal intensity. Most important is the fact that some of the onset temperatures for single element ablations are identical with the onset temperatures for the ablated mixtures (steel, brass), which can be taken as evidence for the fractionation of elements into single element phases.

Influence of the ETV on the Particle Size Distribution (PSD) and the ion signal intensity

After heating the graphite furnace to 2400°C, laser ablation and PSD measurement were initiated simultaneously. Laser ablation and PSD measurement were made at 20°C for 30 s and 60 s, respectively. The ion signals were monitored for the entire time. Heating and cooling cycle times were 5 s (Figure 3).

The temperature was limited to 2400°C because of the large quantity of carbon particles which are released from a graphite furnace at higher temperatures (Figure 10). These particles can severely impact the particle size measurement (PSM) system. Blank measurements at different temperatures were used for background subtraction of the given PSD measurements. The volume of the ablated material was calculated assuming that the particles were spherical. The decrease in the ion signal intensity (ΔI) was calculated as:

$$\Delta I (\%) = 100(I_{2400^\circ\text{C}} - I_{20^\circ\text{C}}) / I_{20^\circ\text{C}}$$

where $I_{2400^\circ\text{C}}$ and $I_{20^\circ\text{C}}$ are the mean intensities measured at 2400°C and 20°C, respectively.

Figure 11 shows the influence of the ETV temperature on the particle size distribution (PSD) for different metals. Gallium is representative of metals that have a low melting point (Ga, Sn, Pb, Cd, and Zn), silver is representative of elements with intermediate melting points (Al, Ag, Au, Cu, Mn, Si, Ni, Co, and Ti), and molybdenum is representative of metals that have high melting points (Mo, W, Pt, and Ta). For the metals with low melting points, a change of the particle size distribution is observed at 2400°C, the temperature at which the small particles are nearly entirely removed from the sample stream and the number of the larger particles is decreased (Figure 11a). For metals with intermediate melting points, a change of PSD was not observed. For these metals, only

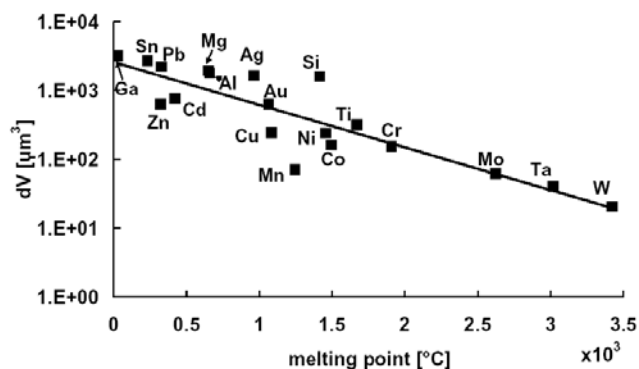


Figure 12. Correlation between change of total particle volume and melting point of metals.

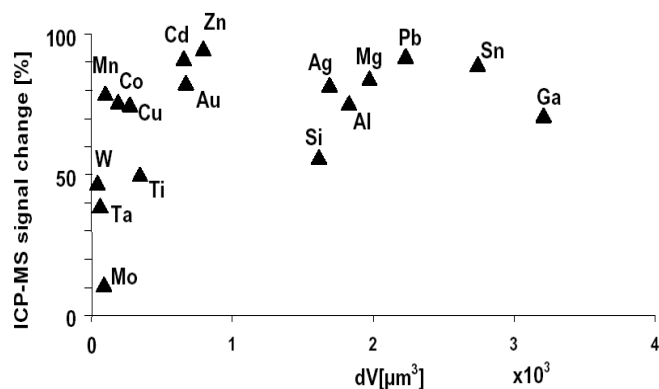


Figure 14. Dependence of the decrease of ICP-MS signal intensity on change of the total volume of the particles

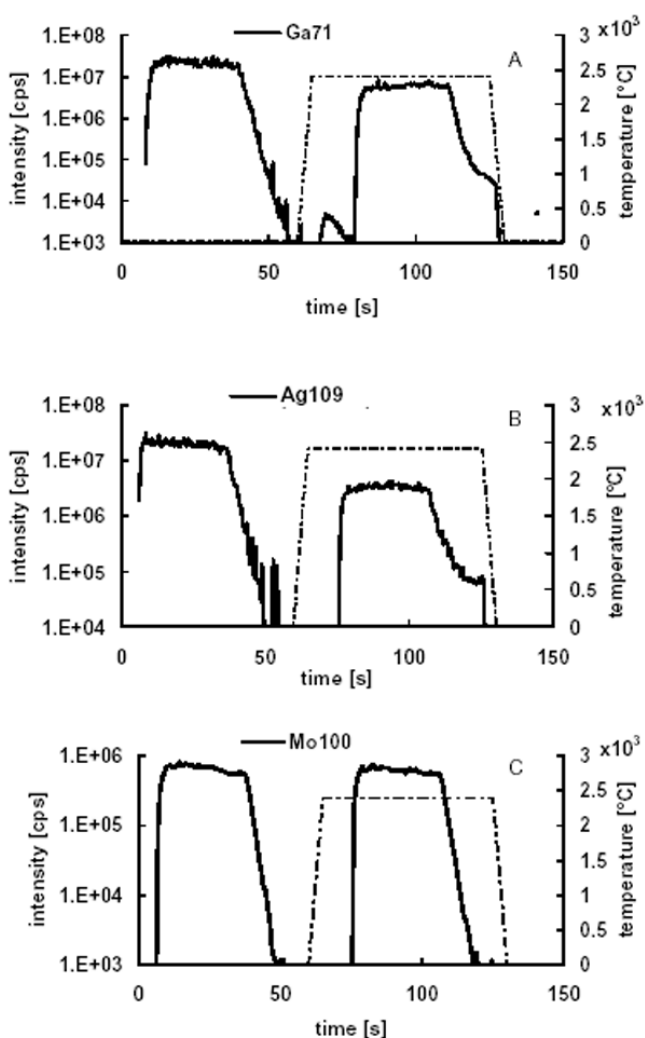


Figure 13. Influence of different ETV temperature on ICP-MS signal intensity of gallium (A), silver (B) and molybdenum (C)

the number of the particles changed (Figure 11b). The PSD and the number of the particles for the high melting metals are not significantly changed by the ETV. These high melting elements produce predominantly smaller particle size (Figure 11c).

The correlation between the change in the total volume of particles as the temperature set on the ETV was changed from 20°C to 2400°C and the melting point of the metals is shown in Figure 12. A decrease in the ion signal at 2400°C is observed relative to that at 20°C (Figure 13). The lack of correlation between the decrease in the ion signal intensity and a change in total particle volume suggests that the ETV influences the total PSD of the low melting metals and not only the fraction of larger particles, which are important for complete ionization in the ICP-MS (Figure 14).

Conclusions

An ETV, installed between a laser ablation cell and an ICP, is a suitable tool to study the composition and high temperature behaviour of laser-induced aerosols. Ablated particulate material evaporates in the graphite furnace, a process which commences when the graphite furnace temperature is approximately 500°C below the boiling point of the element. Vapour is then deposited onto the surface of the furnace tube, and a decrease in the ion intensity results. At a higher ETV temperature, an increase in signal intensity occurs when the sample is released from the surface. This sample release occurs at approximately 2500°C, when the thermal release of the element from the graphite takes place. The presence of a temperature gradient in the ETV simulates that the vaporization of particles within the ICP would also start at different positions within the ICP. However, the slopes

are different and might not be measurable within the ICP.

The start of the decreasing ICP-MS signals measured for brass and steel alloys ablation behaviour is for some elements similar to that of single element material ablations, suggesting that single phase separation takes place within the laser-induced aerosol (*e.g.* Zn in brass). The decreased temperatures for Mn and Ni suggest that they are transported in a Zn-containing phase, while Al, Ag, Sn, and Pb are preferentially found in a Cu phase. In the steel samples, the change in signal intensities of trace components is observed at similar temperature as for the Fe signals. This suggests that the trace components are alloyed with iron in the aerosol.

The total volume of particles transported to the ICP is reduced when using the ETV at 20°C and 2400°C. The reduction in the volume of transported material is correlated with the melting points of the metals. The PSD of low melting point elements is changed with temperature. For metals with intermediate melting points, a reduction was observed in the total particle volume, but the PSD remained unchanged. The initial particle sizes produced by the laser for high melting point metals indicate more small particles, which remain unchanged by the ETV at 2400°C. The PSD of high melting metals are not influenced by temperature, and the total volume of the particles is slightly reduced.

Finally, the important conclusion is that ETV preheating of laser-generated particles is a coarse simulation (at lower temperatures and at different temporal resolution) of processes within the ICP. Even for higher temperature profiles, it becomes understandable that the particle vaporization can occur at different positions within the ICP, and the positions are size and therefore matrix-dependent. Furthermore, the degree of elemental fractionation into individual particle sizes during the ablation process can be determined by comparing signal intensities for single element ablations and their behaviour within different matrices (brass and steel). However, to reduce particle size distributions by ETV before the particles enter the ICP plasma, such a device needs to be directly connected to the ICP-torch. Furthermore, this initial work also showed that selective removal of different elements is possible, which could be useful for the online reduction of interferences in LA-ICP-MS.

Acknowledgements

The authors would like to thank ETH Zurich for supporting this work. TV would like to thank the Erasmus student exchange program at ETH Zurich. Critical reading and comments on the manuscript by two anonymous reviewers and H.P. Longerich is also acknowledged.

References

1. A. Martin-Esteban and B. Slowikowski, *Anal. Chem.*, **33**, 43 (2003).
2. D.E. Nixon, V.A. Fassel and R.N. Kniseley, *Anal. Chem.*, **46**, 210 (1974).
3. R.A. Newman and Z.H. Siddik, *Clinica Chimica Acta*, **179**, 191 (1989).
4. F. Plantikow-Vossgätter and E. Denkhaus, *Spectrochim. Acta B*, **51**, 261 (1996).
5. D. Pozebon, V.L. Dressler and A.J. Curtius, *Talanta*, **51**, 903 (2000).
6. G. Záray and T. Kántor, *Spectrochim. Acta B*, **50**, 489 (1995).
7. G. Galbács, F. Vanhaecke, L. Moens and R. Dams, *Microchemical Journal*, **54**, 272 (1996).
8. N.J. Miller-Ihli and S.A. Baker, *Spectrochim. Acta B*, **56**, 1673 (2001).
9. C. Moor, P. Boll and S. Wiget, *Fresenius' J. Anal. Chem.*, **359**, 404 (1997).
10. W.H. Hinds, D.C. Gregoire and E.A. Ozaki, *J. Anal. At. Spectrom.*, **12**, 131 (1997).
11. D.C. Grégoire and R.E. Sturgeon, *Spectrochim. Acta B*, **54**, 773 (1999).
12. J. Bernhardt, T. Buchkamp, G. Hermann and G. Lasnitschka, *Spectrochim. Acta B*, **55**, 449 (2000).
13. R.E. Russo, X.L. Mao, O.V. Borisov and H. Liu, *J. Anal. At. Spectrom.*, **15**, 1115 (2000).
14. O.V. Borisov, X. Mao and R.E. Russo, *Spectrochim. Acta B*, **55**, 1653 (2000).
15. D. Bleiner and D. Günther, *J. Anal. At. Spectrom.*, **16**, 449 (2001).
16. P. Heszler, *Appl. Surf. Sci.*, **186**, 538 (2002).
17. E. Ozawa, Y. Kawakami and T. Seto, *Scripta Mater.*, **44**, 2279 (2001).
18. N. Koshizaki, A. Narazaki and T. Sasaki, *Scripta Mater.*, **44**, 1925 (2001).
19. Y. Tang and Q. Qin, *Chem. Phys. Lett.*, **343**, 452

- (2001).
20. M. Guillong and D. Günther, *J. Anal. At. Spectrom.*, **17**, 831 (2002).
 21. C.M. Sparks, J.A. Holcombe and T.L. Pinkston, *Appl. Spectrosc.*, **50**, 86 (1996).
 22. M. Guillong, H.R. Kuhn and D. Günther, *Spectrochim. Acta B*, **58**, 211 (2003).
 23. D. Langer and J.A. Holcombe, *Anal. Chem.*, **71**, 582 (1999).